SPECIAL ISSUE ARTICLE

Friction stir processing of 316L stainless steel plate

Y. C. Chen*[1], H. Fujii[1], T. Tsumura[1], Y. Kitagawa[1], K. Nakata[1], K. Ikeuchi[1], K. Matsubayashi[2], Y. Michishita[2], Y. Fujiya[2] and J. Katoh[3]

316L stainless steel plates were friction stir processed using polycrystalline cubic boron nitride tools. Mechanical properties and microstructure evolution of the friction stir processing (FSP) zone were investigated. Tensile test results showed that the tensile strengths of the defect free FSP zones were equal to those of base metals. All the samples fractured at the base metal side. Microstructural observation results showed that the grains in the FSP zone were refined by the tool. The FSP zone was a roughly equiaxed grain structure and the grain size was in the range of 10–30 μm, which was smaller than that in the base metal (30–80 μm). Moreover, transmission electron microscopy observation revealed that sigma phases formed in this zone during FSP.

Keywords: Stainless steel, Friction stir processing, Microstructure, Mechanical properties

Introduction

Austenitic stainless steel, AISI type 316 and its modified grades such as 316L have applications as a structural material in nuclear power plants for the construction of water storage tanks.[1] The choice of this alloy is based on its excellent high temperature tensile and creep fatigue strengths in combination with good fracture toughness and fabricability. As nuclear plants around the world grow older there is an increasing incidence of stress corrosion cracking (SCC) problems.[2] The repair of SCC is becoming an urgent task to extend the service life of stainless steel water storage tanks which have experienced SCC cracks at the external surface.

Friction stir processing (FSP) is an emerging surface engineering technology,[3,4] developed based on the basic principles of friction stir welding (FSW),[5,6] which can provide localised microstructure modification in near surface layers of processed materials. A rotating tool consisting of a shoulder and a pin is plunged into a workpiece and then travels in an expected direction. The tool serves two primary functions, heating and deformation of a material. The material in FSP zone undergoes extreme levels of plastic deformation and thermal exposure, which normally results in significant microstructural refinement and homogeneity of the processed zone, thereby improving strength, wear property, corrosion resistance and so on. The technology of FSP essentially provides a high integrity smooth repair of shallow surface defects. Compared with conventional weld repair methods, this technology can offer advantages for online application particularly in terms of its lower risk of through wall penetration. So far FSP technique has been successfully used for producing the fine grained structure,[7–12] modifying the microstructure of materials,[13–17] and synthesising the intermetallic compound *in situ*.[18] However, considerably less attention has been given to surface repair, despite their significant industrial importance.

In this study, 316L stainless steel plates are friction stir processed using polycrystalline cubic boron nitride tools to investigate the processability of this material using FSP. Microstructure evolution and mechanical properties of the FSP zone are investigated to explore the effect of FSP on the surface properties of the target, for instance, tensile properties, microhardness, microstructure and so on.

Experimental

The base materials were 15 mm thick 316L stainless steel plates. The chemical compositions and mechanical properties of the base materials are shown in Table 1. Rectangular experimental samples, 250 mm long by 200 mm wide, were processed using a FSW machine. After a series of feasibility tests, following experimental parameters were selected. The processing parameters were rotation speeds of 4, 5 and 6 rad s^{-1} and travelling speeds of 0·267, 0·333 and 0·4 mm s^{-1}. The upsetting forces of the FSP tool were 25, 30 and 35 kN. The tool was fabricated from polycrystalline cubic boron nitride and consisted of a convex shoulder having a diameter of 22 mm and a tapered pin. The pin tapered from 9 mm at the shoulder to 4 mm at the pin tip. The shoulder surface had a spiral pattern to enhance the stirring effect. The length of the pin was 5 mm and the processing tilt angle was 0°. To avoid surface oxidation, argon shielding was employed around the tool during FSP.

[1]Joining and Welding Research Institute, Osaka University, Osaka 567 0047, Japan
[2]Manufacturing Technology Centre, Mitsubishi Heavy Industries, Ltd, Takasago 676 8686, Japan
[3]Advanced Nuclear Plant Designing Section, Mitsubishi Heavy Industries, Ltd, Kobe 652 8585, Japan

*Corresponding author, email armstrong@hit.edu.cn

Published by Maney on behalf of the Institute
Received 29 September 2008; accepted 30 October 2008
DOI 10.1179/136217108X386527

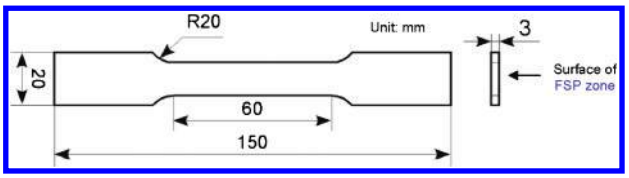

1 Schematic of tensile test specimen

After FSP, the FSP zone was cross-sectioned perpendicular to the FSP direction for the metallographic analyses and tensile tests using an electrical discharge cutting machine. The mechanical properties of the FSP zone were measured using tensile tests. The tensile tests were carried out at room temperature at a crosshead speed of 0·0167 mm s^{-1} using a tensile testing machine, and the mechanical properties of the FSP zone were evaluated using three tensile specimens cutting from the same sample. The shape of the test specimen is shown in Fig. 1. Vickers hardness profiles were measured at 2 mm deep from the surface of the FSP zone under a load of 0·98 N for 15 s along the centrelines of the cross-sections of the samples with the distance between neighbouring measured points being 1 mm. Microstructural observations were performed by optical microscopy, transmission electron microscopy (TEM) and ERA-8800FE scanning electron microscopy (SEM) equipped with an energy dispersive X-ray spectroscopy analysis system. The specimens for optical microscopy were mechanically ground with water abrasive paper and polished with 3 and 1 μm diamond, and etched electrolytically in a solution of 10% oxalic acid + 90% water with a power supply set to 15 V for 90 s. Thin disks for TEM were cut from the various locations of the FSP zone using a focussed ion beam instrument (Hitachi High-Technologies FB-2000A). The thin disks were observed at 200 kV using JEOL JEM-2010 TEM.

Results and discussion

Figure 2 shows a typical appearance and cross-section of an FSP zone processed at processing parameters of 5 rad s^{-1}/0·333 mm s^{-1} and the corresponding X-ray inspection result. It can be seen from this figure that the defect free FSP zone can be obtained when appropriate processing parameters are carried out. The typical stir zone (SZ), thermomechanically affected zone (TMAZ) and base metal (BM) are observed. In this case, the authors are mainly interested in the structure feature in the SZ and observe several characteristic positions

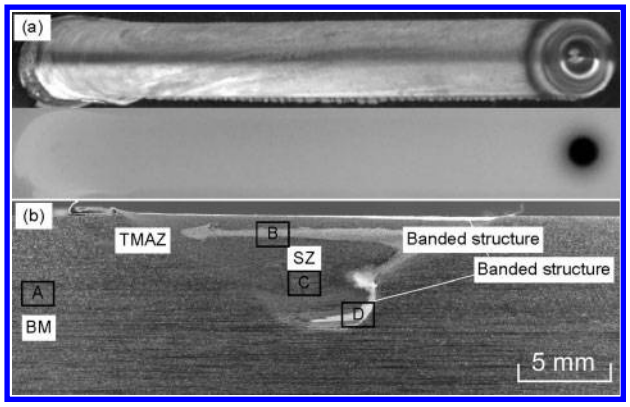

a appearance of FSP zone and X-ray inspection result; *b* cross-section of FSP zone

2 Appearance and cross-section of typical FSP zone

(A, B, C and D shown in Fig. 2*b*). The details of the microstructural variations are demonstrated in Fig. 3. Moreover, it should be noted that banded structures are detected in the SZ. The microstructure in this region is characterised using TEM and the results will be shown later in this study.

Table 2 presents the X-ray inspection results and shows the effect of processing parameters on the FSP formation. From this table we can find that high forge loads, low rotation speeds and travelling speeds tend to form the defect free FSP zone. Under current experimental conditions, the defect free FSP zone can be obtained at the selected rotation speed and travelling speed range when the forge load of 35 kN is employed.

Table 3 shows the tensile test results of the defect free FSP zone. Tensile test results show that the tensile strength of the defect free FSP zone is equal to that of base metal. All the tensile test samples fracture at the base metal side. Figure 4 shows the typical tensile properties, fracture locations and microhardness distributions of the defect free FSP zone. The stress–strain curve shows a typical ductile fracture feature because the tensile test samples fracture at base metal side. It can be seen from Fig. 4*b* that the microhardness in the SZ is slightly higher than that of base metal. The peak value of the microhardness is from the banded structure area.

Figure 3 shows the details of the microstructural variations mentioned in Fig. 2. It can be seen from Fig. 3*a* that the base metal consists of coarsened grain structures in the range of 30–80 μm distributed along the rolling direction. Figure 3*b* shows the microstructure in

Table 1 Chemical compositions and mechanical properties of base materials

	Chemical compositions, mass-%									Mechanical properties	
Base materials	C	Si	Mn	P	S	Ni	Cr	Mo	Fe	Strength, MPa	Elongation, %
316L steel	0·014	0·64	1·18	0·03	0·002	12·11	17·33	2·06	Bal.	545	64

Table 2 Effect of processing parameters on FSP formation

Load	25 kN			30 kN			35 kN		
Speed, mm s^{-1}	0·267	0·333	0·4	0·267	0·333	0·4	0·267	0·333	0·4
Rotation speed A, 6 rad s^{-1}	X	X	X	○	X	X	○	○	○
Rotation speed B, 4 rad s^{-1}	X	X	X	○	○	○	○	○	○

X: FSP zone with void defect; ○: Defect free FSP zone.

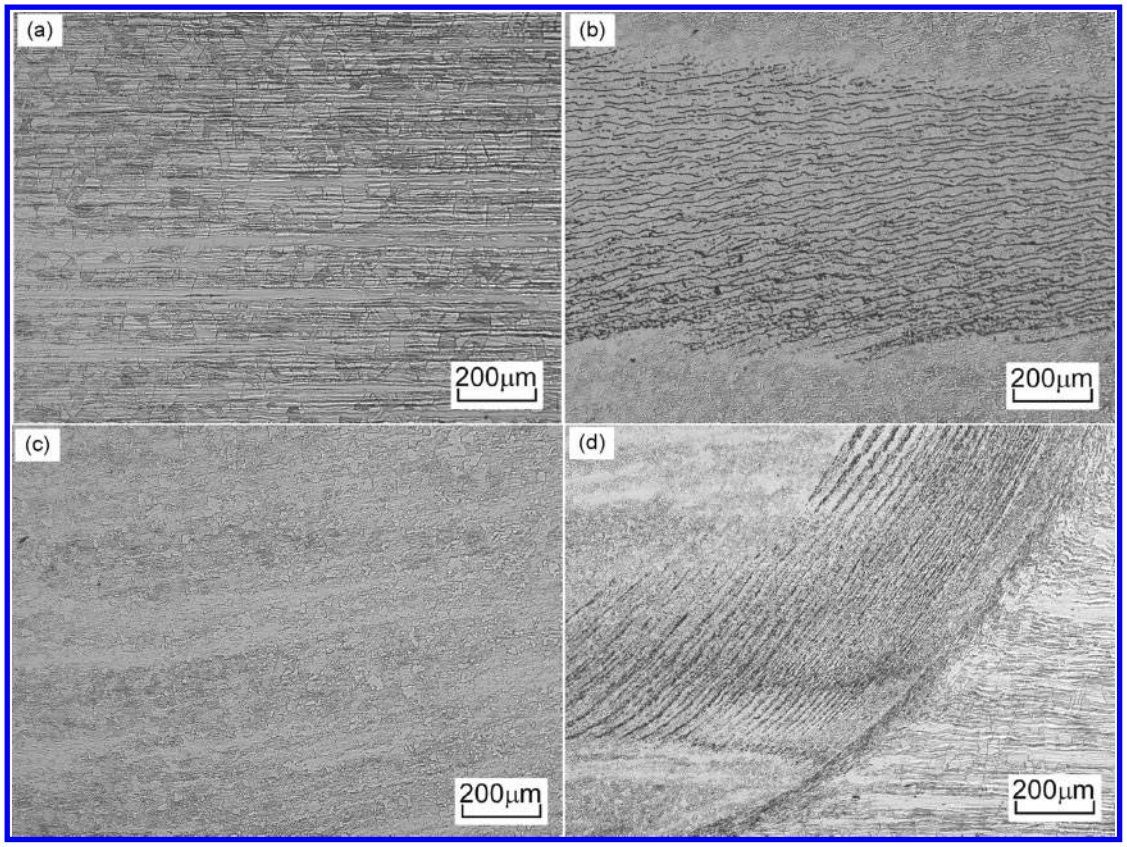

a position A; *b* position B; *c* position C; *d* position D

3 Microstructure of different positions shown in Fig. 2*b*

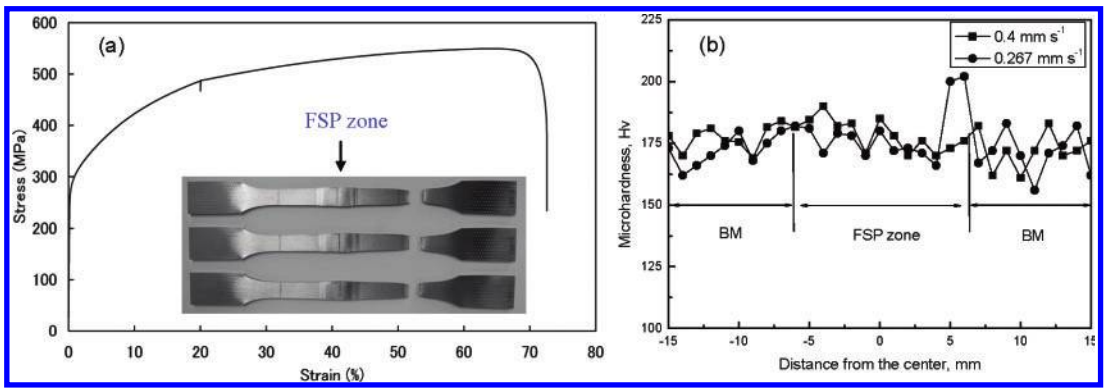

a typical stress–stain curve; *b* microhardness distribution of FSP zone (5 rad s^{-1})

4 Tensile properties and microhardness profiles of FSP zone

the banded area. Lamellar structures are observed in the banded area. It looks like lineal etch pits. Figure 3*c* shows the microstructure in the centre of the SZ. The grains in the SZ are refined by the tool. The SZ shows a roughly equiaxed grain structure and the grain size is in the range of 10–30 μm, which is smaller than that in the BM. Figure 3*d* shows the microstructure at the bottom of the SZ in the advancing side. Lamellar structures similar to those in the banded structure area are found.

Figure 5 shows the SEM micrographs of the banded structure. Figure 5*b* is the high magnification micrograph of Fig. 5*a*. This result clearly shows that the banded structure is a series of shallow lineal etch pits after etching. Energy dispersive X-ray spectroscopy

Table 3 Tensile strengths of the defect free FSP zone*

Load	30 kN			35 kN		
Speed, mm s^{-1}	0·267	0·333	0·4	0·267	0·333	0·4
Rotation speed A, 6 rad s^{-1}	554 Mpa	–	–	546 Mpa	546 Mpa	550 Mpa
Rotation speed B, 4 rad s^{-1}	553 Mpa	557 Mpa	558 Mpa	554 Mpa	557 Mpa	552 Mpa

*: all the defect free FSP zone fractured at base metal side.

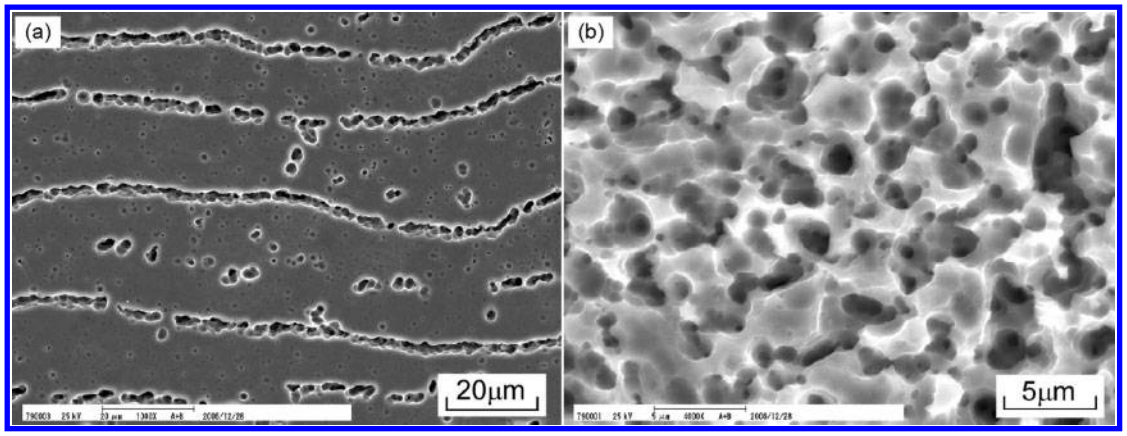

a low magnification; *b* high magnification

5 Images (SEM) of banded structure

analysis results show that the content of Cr in the centre of etch pits is slightly higher than that at the pits border. This result suggests that Cr rich precipitates possibly form in this region, which results in Cr depletion zone around the precipitates. The presence of Cr depletion zone will worsen the corrosion resistance of the banded area. The precipitates in banded structure are observed and characterised by TEM.

Transmission electron microscopy micrographs are shown in Fig. 6. Figure 6*a* indicates that the regions with the banded structure have short rod-like particles with size of 200–300 nm both along the grain boundaries and in the grain interiors. The electron diffraction pattern obtained from the particle A is shown in top right corner of Fig. 6*a*. The electron diffraction pattern reveals that the particle is sigma phase with tetragonal structure. Figure 6*b* shows the dark field image of the TEM morphology of short rod-like particles from the diffraction spot [311].

Sigma phases are first observed in FSW of 304 austenite stainless steel by Park *et al.*[19] In current experiments, the formation of sigma phases is also detected in FSP of 316L austenite stainless steel. In general, sigma phase is formed during aging at temperatures between 773 and 1073 K. The direct decomposition of austenite to sigma phase requires long time due to the accompanying redistribution of alloying elements by substitutional diffusion.[20] However, sigma formation can be accelerated in the duplex microstructure of ferrite and austenite phases and can be significantly accelerated by strain and recrystallisation during aging.[21–23] Since FSW introduces high strain and it accompanies dynamic recrystallisation in the stir zone, Park *et al.*[19,24,25] suggest that the sigma phase can be rapidly formed by the transformation of austenite to delta ferrite at high temperatures and the subsequent decomposition of the ferrite under the high strain and recrystallisation induced by friction stirring. The formation of sigma phase causes Cr depletion in the banded structure. It results in the significant degradation of the corrosion resistance in this region. However, the most attractive aspect for the novel repair technology is that the base material is not melted during friction stir processing. The porosity and grain boundary cracking associated with fusion weld repair technology can be eliminated and the mechanical property of the repair zone can be significantly improved. Moreover, compared with conventional weld repair methods, this technology can offer advantages for online application particularly in terms of its lower risk of through wall penetration. Therefore, friction stir processing repair technology is still a preferred online repair technology.

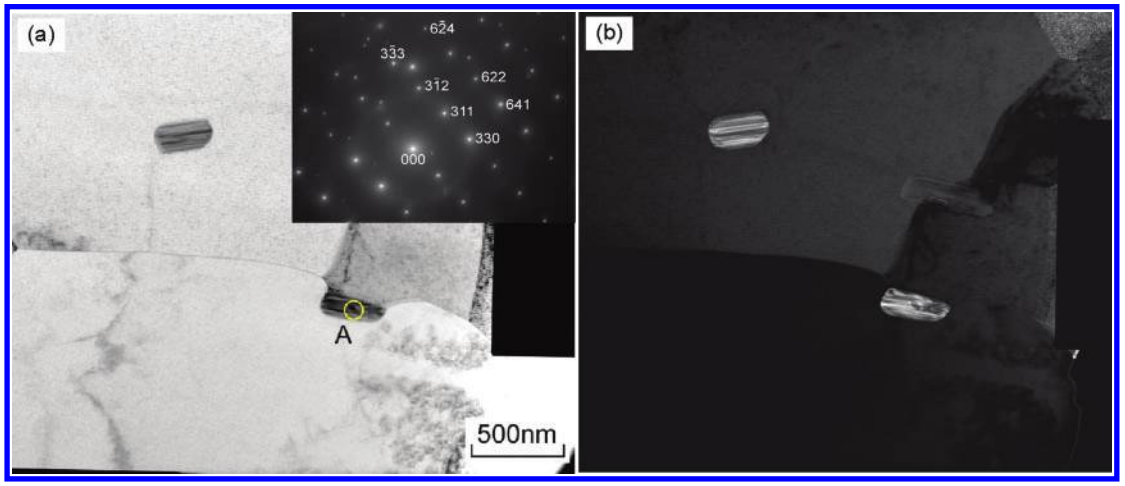

a bright field image; *b* dark field image from diffraction spot [311]

6 Images (TEM) of banded structure

Conclusions

316L stainless steel plates were successfully processed using friction stir processing technology. The microstructure evolution and the mechanical properties of the FSP zone were investigated. The important findings are shown as the following:

The defect free FSP zone could be obtained when appropriate processing parameters were carried out. High forge loads, low rotation speeds and travelling speeds tended to form the defect free FSP zone. In current experimental conditions, the defect free FSP zone could be obtained at selected rotation speed (4–6 rad s^{-1}) and travelling speed (0·267–0·4 mm s^{-1}) range when the forge load of 35 kN was employed. Tensile test results showed that the tensile strengths of the defect free FSP zone were equal to those of the base metals. All the tensile test samples fractured at the base metal side.

The stir zone maintained refined grains and showed a roughly equiaxed grain structure. Meanwhile, sigma phases which caused Cr depletion were detected in the banded structure area of the stir zone. The formation of sigma phases might result in highly degraded corrosion resistance of friction stir surface processing of 316L stainless steel plates.

Acknowledgement

The work was funded by the 'Innovative Nuclear Research and Development Program' of the Ministry of Education, Culture, Sports, Science and Technology (MEXT), Japan.

References

1. Y. Takahashi, H. Shibamoto and K. Inoue: *Nucl. Eng. Design*, 2008, **238**, (2), 310–321.
2. O. M. Alyousif and R. Nishimura: *Corros. Sci.*, 2008, **50**, (8), 2353–2359.
3. R. S. Mishra, M. W. Mahoney, S. X. McFadden, N. A. Mara and A. K. Mukherjee: *Scr. Mater.*, 1999, **42**, (2), 163–168.
4. R. S. Mishra and M. W. Mahoney: *Mater. Sci. Forum*, 2001, **357–359**, 507–514.
5. W. M. Thomas, E. D. Nicholas, J. C. Needham, M. G. Murch, P. Templesmith and C. J. Dawes: 'Friction stir butt welding', G B patent application no. 9125978·8, 1991.
6. R. S. Mishra and Z. Y. Ma: *Mater. Sci. Eng. R*, 2005, **R50**, (1–2), 1–78.
7. J. Q. Shu, T. W. Nelson and C. J. Sterling: *J. Mater. Res.*, 2003, **18**, (8), 1757–1760.
8. Z. Y. Ma and R. S. Mishra: *Scr. Mater.*, 2005, **53**, (1), 75–80.
9. J. Q. Shu, T. W. Nelson and C. J. Sterling: *Scr. Mater.*, 2005, **52**, (2), 135–140.
10. Z. Y. Ma, R. S. Mishra and M. W. Mahoney: *Acta Mater.*, 2002, **50**, (17), 4419–4430.
11. I. Charit and R. S. Mishra: *Mater. Sci. Eng. A*, 2003, **A359**, (1–2), 290–296.
12. C. J. Chang, C. J. Lee and J. C. Huang: *Scr. Mater.*, 2004, **51**, (6), 509–514.
13. K. Nakata, Y. G. Kim, H. Fujii, T. Tsumura and T. Komazaki: *Mater. Sci. Eng. A*, 2006, **A437**, (2), 274–280.
14. D. Zhang, M. Suzuki and K. Maruyama: *Scr. Mater.*, 2005, **52**, (9), 899–903.
15. K. Oh-ishi and T. McNelley: *Metall. Mater. Trans. A*, 2004, **35A**, (9), 2951–2961.
16. K. Oh-ishi and T. McNelley: *Metall. Mater. Trans. A*, 2005, **36A**, (6), 1575–1585.
17. K. Oh-ishi, A. P. Zhilyaev and T. McNelley: *Mater. Sci. Forum*, 2006, **503–504**, 161–168.
18. C. J. Hsu, P. W. Kao and N. J. Ho: *Scr. Mater.*, 2005, **53**, (3), 341–345.
19. S. H. C. Park, Y. S. Sato and H. Kokawa: *Scr. Mater.*, 2003, **49**, (12), 1175–1180.
20. M. Schwind, J. Kallqvist, J. O. Nilsson, J. Agren and H. O. Andren: *Acta Mater.*, 2000, **48**, 2473–2481.
21. J. M. Vitek and S. A. David: *Weld. J.*, 1984, **63**, (8), 246–253.
22. R. A. Farrar: *J. Mater. Sci.*, 1985, **20**, (11), 4215–4231.
23. J. M. Vitek and S. A. David: *Weld. J.*, 1986, **65**, (4), 106.
24. S. H. C. Park, Y. S. Sato, H. Kokawa, K. Okamoto, S. Hirano and M. Inagaki: *Sci. Technol. Weld. Join.*, 2005, **10**, 550–556.
25. R. Nandan, G. G. Roy, T. J. Lienert and T. Debroy: *Sci. Technol. Weld. Join.*, 2006, **11**, (5), 526–537.